Polymorphism of Resorcinol Explored by Complementary Vibrational Spectroscopy (FT-RS, THz-TDS, INS) and First-Principles Solid-State Computations (Plane-Wave DFT)

5 AUTHORS, INCLUDING:

Edward Mikuli
Jagiellonian University

99 PUBLICATIONS   **572** CITATIONS

SEE PROFILE

Norbert Palka
Military University of Technology

119 PUBLICATIONS   **324** CITATIONS

SEE PROFILE

Polymorphism of Resorcinol Explored by Complementary Vibrational Spectroscopy (FT-RS, THz-TDS, INS) and First-Principles Solid-State Computations (Plane-Wave DFT)

Kacper Drużbicki,*[,†,‡,§] Edward Mikuli,[†] Norbert Pałka,[∥] Sławomir Zalewski,[⊥] and Mirosława D. Ossowska-Chruściel[⊥]

[†]Department of Chemical Physics, Faculty of Chemistry, Jagiellonian University, Ingardena 3, 30-060 Cracow, Poland

[‡]Department of Radiospectroscopy, Faculty of Physics, Adam Mickiewicz University, Umultowska 85, 61-614 Poznan, Poland

[§]Frank Laboratory of Neutron Physics, Joint Institute for Nuclear Research, 141980 Dubna, Russian Federation

[∥]Institute of Optoelectronics, Military University of Technology, Gen. S. Kaliskiego 2, 00-908 Warsaw, Poland

[⊥]Department of Technology and Chemical Physics, Institute of Chemistry, University of Natural Sciences and Humanities, 3-go Maja 54, 08-110 Siedlce, Poland

S Supporting Information

ABSTRACT: The polymorphism of resorcinol has been complementary studied by combining Raman, time-domain terahertz, and inelastic neutron scattering spectroscopy with modern solid-state density functional theory (DFT) calculations. The spectral differences, emerging from the temperature-induced structural phase transition, have been successfully interpreted with an emphasis on the low-wavenumber range. The given interpretation is based on the plane-wave DFT computations, providing an excellent overall reproduction of both wavenumbers and intensities and revealing the source of the observed spectral differences. The performance of the generalized gradient approximation (GGA) functionals in prediction of the structural parameters and the vibrational spectra of the normal-pressure polymorphs of resorcinol has been extensively examined. The results show that the standard Perdew, Burke, and Ernzerhof (PBE) approach along with its "hard" revised form tends to be superior if compared to the "soft" GGA approximation.
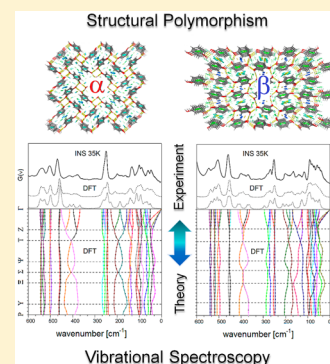
I. INTRODUCTION

The structural polymorphism in pharmaceutical solids is a major problem, since the crystal phase determines the solubility and the bioavailability of drug candidates. Practically, there is no way to predict the extent of polymorphism in any given compound. Thus, it is extremely important to gather the structure–spectrum relation in any kind of applied spectroscopy. Among other techniques, such as solid-state NMR or powder X-ray diffraction, vibrational spectroscopy is considered the method of choice for polymorph screening. While the middle-wavenumber range is commonly used for this purpose, the low-frequency spectral range has been found more relevant as delivering an unambiguous distinction of any possible structural differences in the phases of interest. In fact, most of the studies reported in the contemporary literature are usually focused on marking the spectral differences, while their understanding should be the primary task. In such a case, modern solid-state quantum-chemical calculations can be extremely successful. Currently, density functional perturbation theory (DFPT) has become the state-of-the-art method for studying the vibrational dynamics of condensed matter by pushing out the limits of the static quasi-harmonic approach.

The most prominent spectral differences generally come from the specific interactions driving the phases of interest.

Investigation of the hydrogen bonded molecular crystals is an interesting field of basic research from the point of view of their structure and phase stability. An understanding of the structural transitions in simpler systems is essential to extend the knowledge onto more complex or larger molecular crystals. One of the examples of such model systems is resorcinol (benzene-1,3-diol), which belongs to the group of simple phenols and reveals a rich variety of interesting physical phenomena, such as structural polymorphism or pyro- and piezoelectricity.[1,2] It has found multiple pharmacological applications, serving as an antiseptic or disinfectant as well as being used as a chemical intermediate for production of many other drugs. It is often used in ointments for the treatment of skin diseases such as psoriasis and eczema and applied as an antidandruff agent in various cosmetic products. Under the pills format, the ingredient is served for treatment of gastric ulcers or applied as an analgesic and hemostatic agent. In large doses, it is a poison causing giddiness, deafness, salivation, sweating, and convulsions.[3,4] In addition to its broad medical use, resorcinol has also found a variety of chemical uses for industrial and
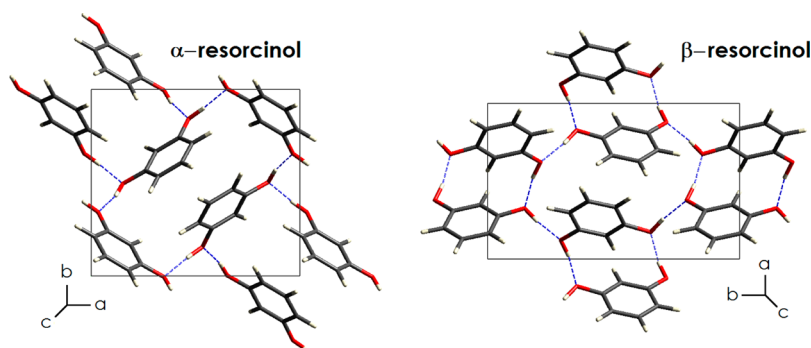
Figure 1. Crystal structure of the α and β polymorphic forms of resorcinol according to Robertson et al.[1,2]

scientific applications. For example, over the past decade, with a rediscovery of banana-shaped liquid-crystalline compounds, resorcinol along with its derivatives was found to be one of the most common central units chosen for the synthesis of the bent-shaped mesogens.[5−8]

Although the history of the structural research of resorcinol started in the 1930s, with the X-ray diffraction studies by Robertson et al.,[1,2] it still attracts the attention as a model organic hydrogen-bonded system. It is known that two phases of resorcinol can be observed at atmospheric pressure, namely, the α- and β-phases, where the α-phase was found to be the equilibrium one (see Figure 1). The β-phase was found to be metastable, progressively transforming to the α-form.

The α-structure was further refined by Bacon, based on neutron single-crystal measurements and delivering the results which were considered to be near the limit of accuracy possible from medium-flux reactors.[9] The neutron studies were finally continued by Bacon using polycrystalline samples and resulting in the most accurate structural data for both structures reported so far.[9−11]

The $\alpha \rightarrow \beta$ phase change is one of the limited number of solid−solid transitions in which the denser phase is stable at a higher temperature and the crystal space group remains the same upon the transformation. Both phases have the same orthorhombic space group $Pna2_1$, with $Z = 4$, while the networks of the hydrogen bonds in the two phases are completely different. The phase transformation is accompanied by the conformational change and subsequent reorganization of the hydrogen-bonding patterns, where the c-axis oriented spiral H-bond network in the α-phase transforms into the a-axis oriented chains in the β-form.

According to Ebisuzaki et al.,[12] the most reliable transition temperature is expected at 369 ± 6 K, being strongly heating rate dependent. The corresponding changes in the enthalpy and entropy were defined as $\Delta H = 1.370 \pm 0.007$ kJ/mol and $\Delta S = 3.71 \pm 0.05$ J/mol·K, respectively.[12] Such a small entropy change is reflected from the fact that the density of vibrational states is not greatly affected, since both forms belong to the same space group and contain the same number of molecules. There is, however, a configurational entropy change for the hydroxyl groups and the change in the crystal packing. Despite such small values of the thermodynamic parameters, the phase change has been classified as a strong first-order-type transformation, where its precursor was studied by Shigenari et al.,[13,14] based on the fluorescence lifetime measurements. It was found that the large-amplitude and short-lived vibrational fluctuations can be suggested as a possible origin of the phase transition precursor.

A lot of attention has already been put into the pressure studies of resorcinol.[12,15−18] Recently, extensive high-pressure X-ray research has been reported by Kichanov et al.[15] No additional phases can be found under the atmospheric conditions, while two other structures exist under high pressure, namely, the γ- and δ-forms. It is known that the $\alpha \rightarrow \beta$ transition tends to be observed upon compression of α-resorcinol at $P \approx 0.5$ GPa;[12,15−17] however, faster pressurization rates suppress the transformation, allowing the α-form to be observed up to nearly $P \approx 3.5$ GPa. Both Rao[17] and Kichanov[15] have observed the $\beta \rightarrow \gamma$ transition at $P = 5.6$ GPa. Unfortunately, the precise information about the structure of the γ-phase remains unknown. Nevertheless, Kichanov et al. have indexed the energy dispersive X-ray diffraction patterns and proposed the orthorhombic $Pnna$ symmetry, with the following $\gamma \approx \beta$ relations between the cell parameters: $a_\gamma \approx a_\beta$, $b_\gamma \approx b_\beta$, and $c_\gamma \approx 2 \times c_\beta$.[15] The authors have concluded that the γ crystal structure can be described as a β-superstructure with the c-constant doubled, implying a possible reorientation of the molecules. Rapid pressurization of α-resorcinol, with the suppression of the $\alpha \rightarrow \beta$ transition, leads to a new phase δ, found above 3 GPa, which, unlike the γ-phase, turns out to be more ordered under comparable pressure conditions.[17] Transitions to the δ- and γ-phases are both described as reversible, suggesting that particular phases are structurally related. In the δ-phase, the occurrence of a stacked configuration is expected according to the observed excimeric luminescence.[17]

Along with the structural aspects, the vibrational spectroscopy of resorcinol has been under debate for many years. The Raman spectrum of α-resorcinol was initially studied at room temperature by Penot and Mathieu,[19] while the infrared spectrum was reported by Hidalgo and Otero.[20] These studies were found however to conflict with the later assignments of phenol and its meta-substituted derivatives proposed by Green et al.[21,22] Finally, the up-to-date data of the molecular vibrations in α-resorcinol were reported by Tripathi,[23] based on the low-temperature infrared and Raman measurements. Raman spectroscopy was further used by Ebisuzaki[12] in order to study the temperature induced $\alpha \rightarrow \beta$ transition, concluding that most of the vibrations remain continuous in both phases. The same conclusion was later drawn by Shigenari et al.,[14] who claimed that there must be some short-lived, local fluctuations of some librational modes, which could be detected by fluorescence spectroscopy, rather than long-wavelength soft modes, since no pretransition effects could be observed with Raman spectroscopy. Nevertheless, the authors were unable to

assign the discussed modes. In the present paper, we would like to shed more light on their findings.

As in the case of the structure, a very strong impact has also been given to the Raman spectroscopy of the pressure-induced transitions.[15−18] Furthermore, resorcinol has been probed by Kleinermanns et al. at the molecular level by means of resonance-enhanced multiphoton ionization (REMPI) and hole burning spectroscopy.[24] The conformational space was also further explored by dispersed fluorescence spectroscopy of the jet-cooled resorcinol.[25] The authors have supported their studies with Hartree−Fock and DFT computations.

Despite the wealth of information gathered, there are, however, no reports of the *ab initio* studies of the structure and vibrational dynamics of both normal-pressure phases of the discussed system. The main goal of this paper is hence to shed more light on the polymorphism−spectrum relation, based on the modern solid-state density functional theory approach. Moreover, we would like to validate the DFPT method for the prediction of the vibrational spectra in the middle-strength hydrogen bonded molecular crystals, based on the example of the discussed structures. For the first time, the vibrational spectra including Raman, time-domain terahertz (TDs-THz), and inelastic neutron scattering (INS) are reported simultaneously for both phases and discussed in detail by referring to the first-principles computations. In addition, we turn to the previously reported pressure-dependent data,[15−18] in order to test the performance of the quoted approach in prediction of the structural properties under pressure.

II. EXPERIMENTAL AND COMPUTATIONAL DETAILS

Sample. The polycrystalline resorcinol (α-phase) with a purity of ~99% was used in all the subsequent measurements. The phase polymorphism of the sample was confirmed, both upon heating and cooling, using differential scanning calorimetry (DSC) at a scan speed of 2 K/min. The measurements of the 21 mg sample were performed in the temperature range 243−380 K, with a Mettler Toledo 822^e DSC Calorimeter. The $\alpha \rightarrow \beta$ transition onset temperature was found at 366.2 K, matching with the data reported by Ebisuzaki et al.[12]

Fourier-Transform Raman Spectroscopy (FT-RS). The temperature-dependent Fourier-transform Raman spectroscopy measurements were performed in the wavenumber range 4000−50 cm^{-1} using a Bruker RamScope III spectrometer, equipped with a 1064 nm excitation line of a Nd:YAG laser and a germanium detector. The laser power of 100 mW, spectral resolution of 2 cm^{-1}, and accumulation of 128 scans were chosen as the experimental conditions. The measurements were performed over the temperature range 238−378 K as covering the $\alpha \rightarrow \beta$ transition. The temperature influence was probed every 10 K at a heating/cooling rate of 5 K/min, by controlling the temperature with a Linkam 600 heating stage.

Time-Domain Terahertz Spectroscopy (THz-TDS). The time-domain terahertz spectroscopy studies were performed in the transmission mode with a Teraview TPS 3000 unit, equipped with a variable temperature sample holder. The quoted setup works with the pulses generated by the 800 nm line of a Ti:sapphire femtosecond laser. The ultrashort laser beam is split into the pump and probe beams and directed throughout the system of mirrors to the emitter and detector, which are both based on the low-temperature grown GaAs dipole antennas. The pump beam is focused on the biased emitter antenna to generate the THz pulses through the

photoconductive phenomenon. Such pulses last near 1 ps and have the broadband spectrum, which usually covers the range of ~3−100 cm^{-1}. The sample was ground using a mortar and pestle in order to reduce the particle size and avoid the scattering loss. A mixture containing 10% of resorcinol and 90% of a high-density polyethylene (HDPE) was prepared to obtain a 400 mg pellet. A pure polyethylene sample was used as a reference. The spectra were collected every 2 K through the temperature range 298−378 K, with a heating/cooling rate of 2 K/min and accumulation of 900 scans per spectrum.

Inelastic Neutron Scattering (INS). The inelastic neutron scattering measurements were performed using a time-of-flight inverted geometry spectrometer NERA, set at the IBR-2 high flux pulsed nuclear reactor at the JINR Dubna, Russian Federation.[26] The incident neutron energies were determined by measuring the neutron time-of-flight across the 109.05 m distance from the IBR-2 water moderator to the sample. The INS spectra were recorded simultaneously for all wavelengths/energies at the scattering angles between 20 and 160°. The energy of the scattered neutrons was selected by cooled beryllium filters and pyrolytic graphite neutron wavelength analyzers. The INS spectrum was registered at the final energy of the scattered neutrons, fixed by the crystal analyzers and beryllium filters at E_f = 4.65 meV. The β-phase was prepared by heating the α-phase sample at 373 K for half an hour. The ~5 g samples were measured for 8 h at 35 K.

Computational Details. Density functional theory calculations in periodic boundary conditions (PBC) were carried out using the plane-wave/pseudopotential method implemented in CASTEP version 6.1.[27] Exchange and correlation were defined with several generalized gradient approximation (GGA) type functionals as discussed further on. It should be strongly emphasized that the computations were performed with very high numerical accuracy, which is essential for the low-wavenumber-range calculations. Designed nonlocal norm-conserving pseudopotentials[28] were used along with the 1200 eV plane-wave kinetic energy cutoff. The k-point grid was kept to maintain a spacing of 0.05 Å^{-1}. The convergence criteria for the total energy, forces, stress, ionic displacement, and SCF iterations were set as 1×10^{-10} eV/atom, 1×10^{-5} eV/Å, 1×10^{-5} GPa, 1×10^{-6} Å, and 5×10^{-12} eV/atom, respectively.

In the constant-volume calculations, the equilibrium structures were obtained by relaxing the delocalized internal coordinates[29] while keeping the experimental cell parameters fixed.[9−11] In the case of the constant-pressure calculations, both ionic coordinates and cell parameters were optimized with semiempirical van der Waals corrections, using a limited-memory Broyden−Fletcher−Goldfarb−Shanno (LBFGS) algorithm, with the three-point finite basis set correction to the energy and stress upon the change of the cell volume.

The phonon frequencies were obtained by diagonalization of the dynamical matrices computed using density functional perturbation theory (linear-response/DFPT).[30−36] The analysis of the resulting eigenvectors was used in a tentative assignment of the computed phonons. The Raman activity tensors were calculated using the hybrid finite displacement/linear-response method in the presence of an external field[37] and finally transformed into the Raman intensities, by taking into account the excitation line and the thermodynamic conditions. For the frequencies computed at the zero wavevector, the acoustic sum rule (ASR) was applied. In addition to the direct evaluation of frequencies and intensities at the Γ-point, the phonon dispersion relations were calculated along the high symmetry

`Article`

Table 1. Cell Parameters of α- and β-Resorcinol as Seen by X-ray[1,2] and Neutron Diffraction (ND)[9−11] along with the Theoretical Plane-Wave DFT Calculations (Present Work)[a]

phase	α-resorcinol				β-resorcinol			
cell parameter	a (Å)	b (Å)	c (Å)	V (Å)	a (Å)	b (Å)	c (Å)	V (Å³)
X-ray diff. (α; β = H) [283−303 K]	10.516(1)	9.541(1)	5.660(1)	567.986	7.91(1)	12.57(2)	5.50(1)	546.858
ND (α = H; β = D) [283−303 K]	10.53(3)	9.53(3)	5.60(2)	567.886	7.934(2)	12.606(2)	5.511(1)	551.188
ND (α; β = D) [4.2 K]	10.447(1)	9.356(1)	5.665(1)	553.709	7.811(1)	12.615(1)	5.427(1)	534.754
DFT PBE-TS (α; β = H) [0 K]	10.370	9.391	5.599	545.244	7.704	12.540	5.433	524.932
DFT PBE-D2 (α; β = H) [0 K]	10.324	9.067	5.621	526.150	7.747	12.463	5.371	518.538
DFT PW91-OBS (α; β = H) [0 K]	10.165	8.512	5.584	483.142	7.022	12.363	5.297	459.874
DFT PBEsol (α; β = H) [0 K]	10.537	9.848	5.701	591.586	7.940	11.995	6.389	608.490
DFT WC (α; β = H) [0 K]	10.626	9.609	5.791	591.291	7.946	11.749	6.954	649.208
DFT PBE (α; β = H) [0 K]	10.936	9.8805	5.843	631.355	8.181	12.078	6.795	671.415
DFT PW91 (α; β = H) [0 K]	10.933	9.884	5.854	632.594	8.156	11.987	6.920	676.541
DFT rPBE (α; β = H) [0 K]	11.454	10.369	6.175	733.383	8.608	12.276	7.242	765.275

[a]The corresponding temperatures are given in K, while H and D stand for the hydrogen and deuterium, respectively.

paths throughout the Brillouin zone. For this purpose, the dynamical matrices were computed on a regular grid of wavevectors and Fourier interpolation was used to extend the computed grid to a desired fine set of points along the high-symmetry directions.[38] From the computed eigenfrequencies and eigenvectors, the inelastic neutron scattering fundamental intensities were predicted with the help of the aClimax program.[39] In order to draw some conclusions on the influence of semiempirical dispersion corrections on the INS spectrum, the finite-displacement phonon calculations were performed at the Γ-point, overcoming the limitations of the present implementation of the linear-response approach.

In order to check the consistency of the plane-wave calculations, the fixed-cell full-electronic periodic calculations were performed using the CRYSTAL09 code at the PBE/pob-TZVP level of theory.[40−43] The convergence criteria were modified to set the root-mean-square of the maximum gradient and the maximum displacement to be equal to 5×10^{-6} and 1.5×10^{-5} Å, respectively. The truncation criterion for the bielectronic integrals was set to 8 8 8 16, while the DFT integration grid was defined as XL. The total energy convergence in the geometry optimization was set to $\Delta E < 1 \times 10^{-9}$, while the SCF energy was calculated with an accuracy of 1×10^{-13} Ha. The k-point electronic sampling was controlled by including 125 points in the irreducible Brillouin zone.

Additionally, the isolated molecule PBE/def2-TZVP[41,42] computations were performed with a "tight" convergence criteria as defined in Gaussian 09, rev. D.1.[44] In order to support the mode assignment, the normal-mode analysis was performed with the help of the GAR2PED program, based on the set of nonredundant local-symmetry coordinates.[45]

III. RESULTS

Structural Properties. As the structure of both polymorphic forms has been studied for many decades, the collected information provides a good reference for a theoretical benchmark study. Here, the structural properties of the α- and β-phases are explored by employing solid-state GGA calculations, which, however, deserve an introduction. An extensive description of the semilocal exchange-correlation functionals for periodic DFT calculations has been already delivered by Haas et al. in ref 46. The GGA developed by Perdew, Burke, and Ernzerhof (PBE) is considered as the standard one in calculations of solids.[41,42] Recently, several new

functionals have been proposed, which (on average) improve the computations of the lattice constants and bulk moduli of solids if compared to the LDA (local density approximation) and PBE approach. In this work, along with standard PBE or PW91 (which may be generally regarded as equivalent), we have tested their revised forms, classified by Haas et al.[46] as "soft" and "hard" GGAs. The "soft" GGAs, namely, Wu and Cohen (WC)[47] and PBE for solids (PBEsol),[48] have an exchange enhancement factor $F_x(s)$ that increases more slowly with the reduced density gradients than PBE, and may be hence regarded as closer to the LDA. In the opposite, we may find a "hard", revised PBE (rPBE),[49] where the enhancement factor rises more rapidly. Nevertheless, the accuracy that can be reached with a GGA functional is somehow limited due to a rather simple mathematical form, depending only on the electron density ρ and its derivative $\nabla\rho$.

Another problem in calculations of molecular crystals is associated with the van der Waals (vdW) forces treatment, which are generally related to the long-range electron correlation effects, being notoriously absent from the local and semilocal density functionals. This explains the incorrect asymptotic behavior of the interaction energy between nonpolar systems. Such behavior leads to a significant deviation in predicted cell constants. So far, several semiempirical schemes for vdW corrections have been developed. An important advantage of the semiempirical vdW corrections is a relatively low request of computational time if compared to the accurate post-Hartree−Fock or quantum Monte Carlo (QMC) methods. An interesting review of the dispersion-correction schemes, classified in analogy with the "Jacob's ladder", has appeared in ref 50. In the present paper, we report the results obtained with an inclusion of the vdW corrections proposed by Ortmann, Bechstedt, and Schmidt for PW91 (PW91-OBS),[51] as well as with the DFT-D2 (G06) scheme proposed by Grimme,[52] and finally, with the use of the Tkatchenko−Scheffler (PBE-TS)[53] corrections to PBE. In the quoted methods, the dispersion correction of the form $E_{ij} = f(R_{ij}) \times C_6^{ij} \times R_{ij}^{-6}$ is added to the DFT total energy for each pair (ij) of atoms, separated by a distance R_{ij}^{-6}. The function $f(R_{ij})$ is a damping function, which is necessary to avoid a divergence for small values of R, while C_6^{ij} is the dispersion coefficient for a pair of atoms. The quoted approaches use slightly different damping functions. Furthermore, the C_6^{ij} coefficients in the Grimme and OBS methods depend only on the chemical species, while, in the TS scheme, the
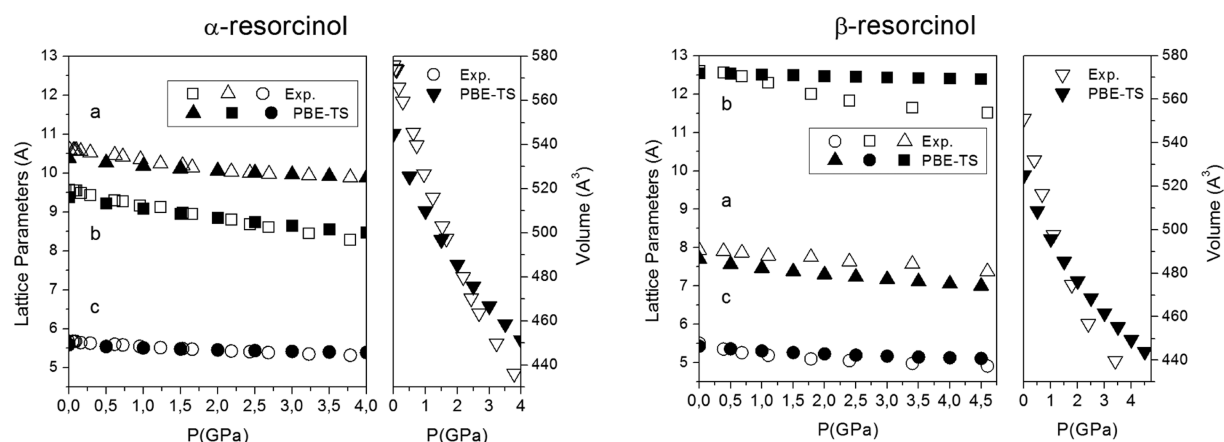
Figure 2. Pressure dependence of the unit cell parameters and the cell volume of α- and β-resorcinol as predicted by PBE-TS calculations and observed experimentally.[15]
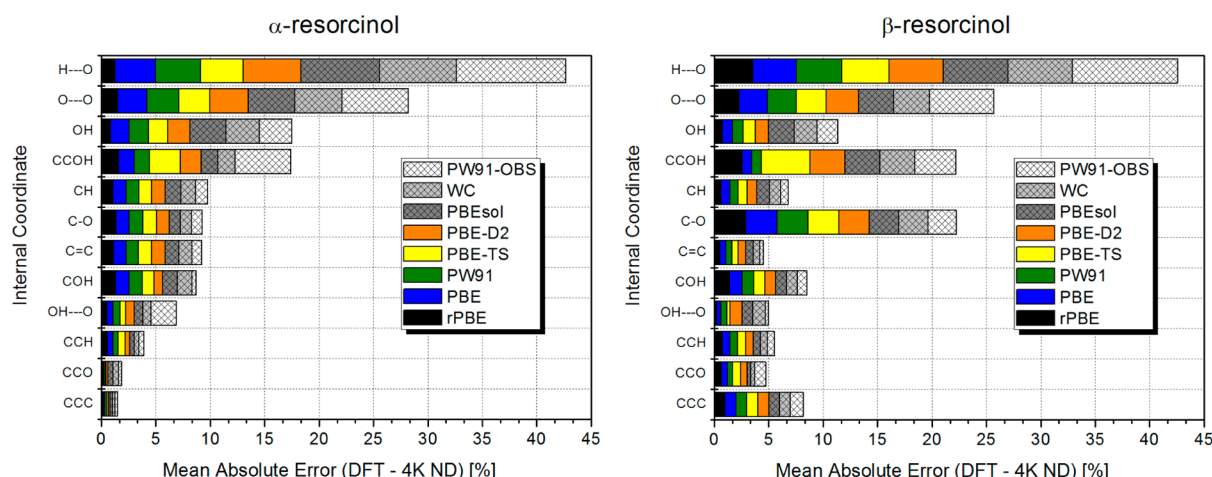

Figure 3. Mean absolute errors (in %) between the experimental internal coordinates of α- and β-resorcinol and the results of the plane-wave DFT calculations (at the low-temperature cell constants/or fully optimized with vdW corrections—D2, TS).[9−11]

coefficients are calculated *on-the-fly* by scaling the free-atom values using Hirshfeld atomic volumes, therefore factoring in the effect of the chemical environment.

The ability of the solid-state DFT calculations to model the cell parameters of resorcinol polymorphs is presented in Table 1 by referring to the experimental data reported from X-ray[1,2] and neutron diffraction (ND).[9−11] Since the theoretical static calculations are performed at 0 K, one should compare the results with the ND data recorded at 4.2 K.

As mentioned above, the $\alpha \rightarrow \beta$ transition is one of the unique transformations in which the high-temperature phase is the denser one. According to the experimental data, the cell volume of the β-structure is slightly lower. In line with the ND results, the difference is ~19 and ~17 Å^3 if referring to the 4.2 and 298 K data, respectively. The phase transition results in shrinking of the *a*-constant and elongation of the *b*-length, while the *c*-parameter remains only slightly perturbed. By analyzing the deviations of the computed cell parameters, one may clearly observe the following tendency: "hard" GGA > PBE > "soft" GGA > GGA-vdW. While the tendency is clearly revealed in the case of the α-phase, it is not so striking for the β-structure. In general, the "hard" GGA (rPBE) completely fails with a strong cell expansion tendency, reaching an extreme deviation of 30% in the case of the *c*-constant in the β-phase. The average errors of 9.8 and 15.4% (*b*) in both phases were

found for the remaining constants. As expected, PBE and PW91 act very similarly and slightly better (PBE = 4.5 (α) and 11.4% (β); PW91 = 4.5 (α) and 12.3% (β)). When turning into the "soft" GGA, a noticeable improvement is observed only for the α-polymorph (WC = 2.2 (α) and 12.2% (β); PBEsol = 2.3 (α) and 8.1% (β)).

A proper cell description can only be achieved with inclusion of the vdW corrections. Among the tested schemes, the standard Grimme's corrections (D2) along with OBS clearly underestimate the cell constants (PBE-D2 = −1.7 (α) and −4.5% (β); PW91-OBS = −1.0 (α) and −4.8% (β)). An excellent performance of the Tkatchenko−Scheffler corrections should be highlighted here, since the PBE-TS outranks any other approach by reducing the mean errors down to −0.7% in both phases. It may be expected that the performance of the TS scheme may go even better with inclusion of the many-body terms,[54] as has been recently shown in ref 55. However, the many-body scheme is not yet available for the applied methodology.

Since PBE-TS can be considered as the method of choice in the calculations of the cell parameters, we may perform the analysis of the pressure-dependent data, referring to the extensive research performed by Kichanov et al.[15] Figure 2 presents the pressure-driven changes of the cell parameters and volume in both polymorphs against the theoretical values

Table 2. Calculated Energy Difference between α- and β-Resorcinol as Derived from the Γ-Point Vibrational Analysis for a Particular Exchange-Correlation Functional (XC)^a

XC	ΔH^{373K} (kJ/mol)	$\Delta E_{lattice}$ (kJ/mol)	ΔE_{ZPE} (kJ/mol)	ΔE_{VIB}^{373K} (kJ/mol)	$\Delta E_{ZPE} + \Delta E_{VIB}^{373K}$ (kJ/mol)	ΔS^{373K} (J/mol·K)
			$\Delta\ (\alpha - \beta)$			
rPBE^{4K}	−4.96	−4.88	0.33	−0.41	−0.08	−6.23
PBE^{4K}	−6.09	−6.15	0.48	−0.41	0.06	−6.51
PW91^{4K}	−6.47	−6.55	0.51	−0.43	0.08	−6.82
PBEsol^{4K}	−7.19	−7.28	0.58	−0.49	0.09	−6.36
WC^{4K}	−8.00	−8.05	0.52	−0.47	0.05	−6.30
PBE-TS^{0K}	−0.97	−0.95	0.27	−0.29	−0.02	−4.16
PBE-D2^{0K}	−4.65	−4.59	0.46	−0.51	−0.06	−7.16
PW91-OBS^{0K}	0.63	−0.03	−0.32	−0.28	−0.60	−4.28
rPBE^{298K}	−3.34	−3.45	0.64	−0.42	0.22	−8.17
PBE^{298K}	−4.44	−4.63	0.72	−0.41	0.30	−7.32
PW91^{298K}	−4.80	−5.00	0.73	−0.42	0.31	−7.61
PBEsol^{298K}	−6.45	−6.55	0.60	−0.39	0.10	−6.98
WC^{298K}	−6.85	−6.92	0.54	−0.38	0.16	−7.10

^{a}The $\alpha - \beta$ difference is given for the calculated enthalpy (ΔH), binding energy ($\Delta E_{lattice}$), zero-point energy (ΔE_{ZPE}), thermal vibrational contribution to enthalpy (ΔE_{vib}^{373K}), and entropy (ΔS^{373K}). The calculations were performed both at fixed (superscript 4K; 298 K ND data) and fully optimized cells (superscript 0K).

predicted by PBE-TS (0 K). Even at the high pressure, the deviations from the predicted parameters do not exceed 3%, except for the b-constant in the β-phase, which is found to shrink more easily. We may hence conclude that PBE-TS may be recommended for a reliable estimation of the cell constants, for instance, when the low-temperature experimental data are missing but needed.

Nevertheless, it is more interesting to examine the performance of the quoted methodology in description of the internal coordinates, which are directly associated with the vibrational spectroscopy and the force constants. Most often, the solid-state calculations are performed with constraints, by keeping the experimentally derived cell parameters fixed, as this data may be routinely obtained from the X-ray measurements. The results of the theoretical calculations are collected against the results of the neutron diffraction data[9−11] in Figure 3.

When analyzing the quoted results, one may observe a reversed tendency. While the "hard" GGA completely fails in description of the cell parameters, it provides the least errors for the molecular coordinates. Such an effect can be associated with an occurrence of significant internal stress, which compensates for the errors due to the deficiencies of the applied methodology. In general, smaller errors were found for the α-structure. These errors in bond lengths do not exceed 2% for rPBE and PBE. The largest errors were found in the C=O bond description, as the error reaches 3.8% in the β-phase (rPBE). The more prominent divergence may be found in the case of the H-bond related parameters, where the quoted tendency is more transparent, especially if focusing on the bond lengths, which are the most critical parameters here. In this case, rPBE beats in quality any other approach, as, for example, the O−H length is predicted with an error smaller than 1% (while with the "soft" GGA errors they are exceeding 3%). The biggest discrepancy was found for the O···H distances. The inclusion of the vdW corrections allows one to achieve an accuracy similar to standard PBE (or PW91). A slightly better performance of the TS scheme was found with respect to the Grimme corrections. One may also note that the OBS corrections are ruining the description of the internal coordinates. Hence, we may conclude that the occurring error scale may be given as follows: rPBE < PBE ≈ PW91 ≈

PBE-D < WC ≈ PBEsol < PW91-OBS. As in the case of the cell-constants prediction, such a hierarchy is not so clear for the β-polymorph.

In order to probe the thermodynamic properties of the studied phases, we have followed the procedure proposed by Rivera et al., which has been earlier presented for an example of the α- and γ-forms of glycine.[56] To a first approximation, the enthalpy difference of two polymorphic modifications may be expressed as the lattice energy difference plus the difference in the vibrational contributions to the enthalpy, that is, $\Delta H = \Delta E_{lattice} + [\Delta E_{ZPE} + \Delta E_{vib}(T)]$, where the negligible PV difference term has been omitted. We have computed both terms by using the sets of the zone-center vibrational states, referring to 373.00 K, which falls on the range of the β-phase stability. The lattice energy of each phase was calculated with respect to the fully optimized C_{2v} (α) and C_s (β) conformers via the molecule-in-a-box ($15 \times 15 \times 15$ Å^3) methodology. All of the energy difference values ($\alpha - \beta$) are collected in Table 2 as given per molecule.

The precise experimental enthalpy of the transition, reported by Ebisuzaki et al.[12] and Bret-Dibat et al.,[57] equals 1.37 (at 369.00 K) and 1.20 kJ/mol (at 366.75 K), respectively, indicating that the thermodynamic effect is extremely small. One may try to roughly estimate the theoretical value of the enthalpy by using the results delivered by each functional. It was generally found that, while the β-phase related conformation for the isolated molecule is that of the lowest energy (ΔEnergy ($\alpha - \beta$) = ∼0.15−0.23 kJ/mol), the total energy of the α-phase structure is lower. Thus, the α-phase binding energy was found to be significantly larger than that for the β-structure. In accordance to Rivera et al.,[56] we have also found that the variation with functional results in very large uncertainties in the lattice energy calculations.

As one may see in Table 2, the binding-energy stabilization of the α-phase is significantly increasing when going from "hard" to "soft" GGA. By comparing the data, derived from the calculations performed both at room- and low-temperature cell constants, one may note a significant lowering of the lattice energy difference due to the cell expansion. The estimated vibrational difference term $[\Delta E_{ZPE} + \Delta E_{VIB(T)}]$ is very small if compared to the lattice-energy difference. The phonons
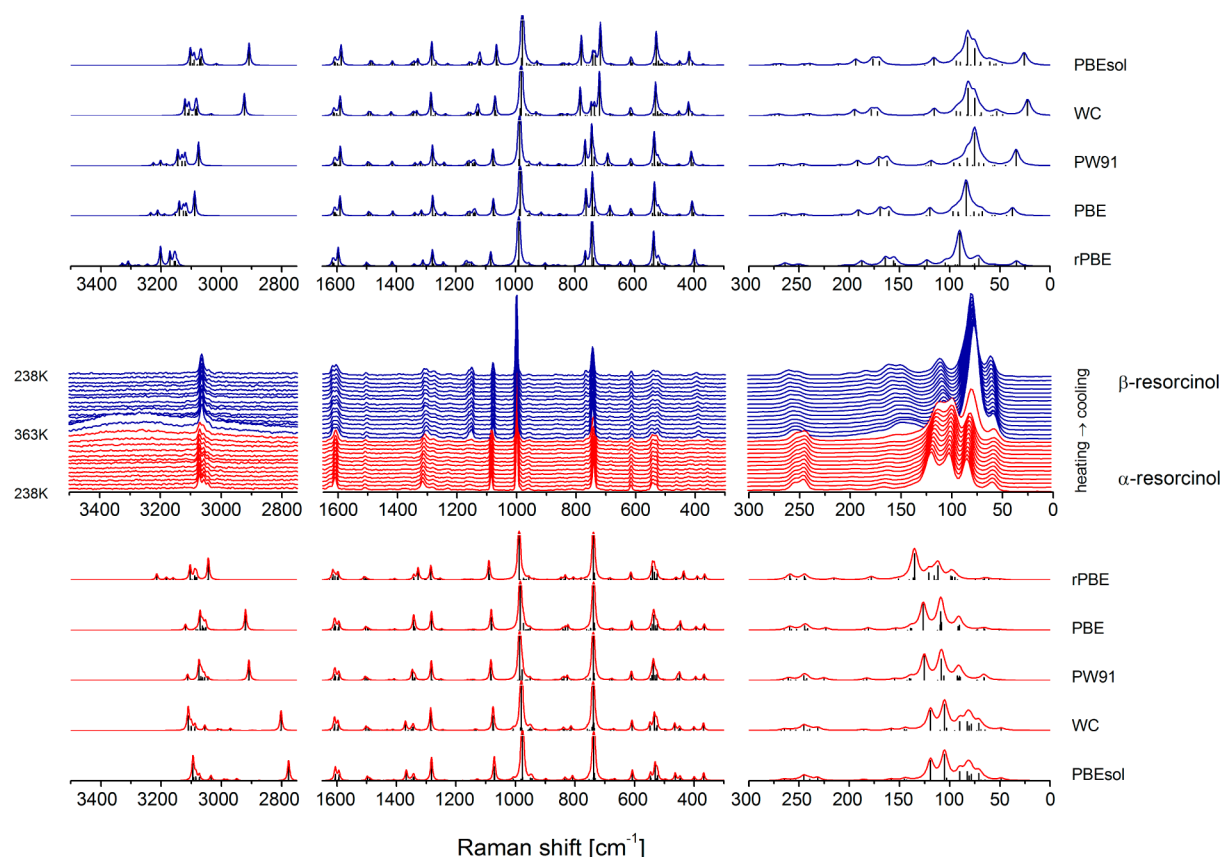
Figure 4. Experimental (middle) temperature-dependent FT-RS spectra of resorcinol, presented against the results of the theoretical calculations (CASTEP/DFT/1200 eV) for the α (bottom) and β (top) polymorphs. The theoretical spectra were computed at the room-temperature cell constants, with use of multiple GGA exchange-correlation functionals.

calculated using the room-temperature cell constants are generally shifted toward higher wavenumbers, which results in greater ZPE and $\Delta E_{VIB}(T)$ contributions. While the ZPE contributions in the α-phase dominate over the β-form, the greater thermal vibrational contribution for the high temperature phase cancels out this effect. One may also note some similarity in performance of rPBE with respect to Grimme's corrected PBE.

Finally, the comparison of the estimated enthalpy values shows that only in the case of the PBE-TS calculations we were able to obtain the value of $\Delta H = 0.97$ kJ/mol, which is on the order of magnitude comparable to the data reported by Ebisuzaki et al.[12] and Bret-Dibat et al.[57] In the remaining cases, the resulting data significantly exceed that value. Furthermore, one may also notice that, while the remaining approaches fail in estimation of the entropy difference, the PBE-TS calculations give a reasonable value of $\Delta S = 4.16$ J/mol·K, which is also close to the experimental values of 3.71 and 3.30 J/mol·K.[12,57]

Vibrational Analysis. The unit cell in both phases contains four molecules, which leads to the 165 optical active phonons, distributed along the symmetry species as follows: $\Gamma_{optical} = 41B_1 + 41B_2 + 41A_1 + 41A_2$. Among the representation, 144 modes are the intramolecular ones, while 21 vibrations ($\Gamma_{external} = 5B_1 + 5B_2 + 5A_1 + 5A_2$) are the external modes. All the symmetry species are Raman active, while the A_2 species are infrared/terahertz forbidden.

In the present work, we have based our discussion on the Raman and inelastic neutron scattering studies, while the low-

wavenumber range has been further supported by the time-domain terahertz spectroscopy.

The INS intensity, $S(Q, \omega_i)$, of the ith mode is proportional to the factor

$$S(Q, \omega_i) \propto Q^2 U_i^2 \exp(-Q^2 U_{i\,total}^2) \sigma_{inc} \tag{1}$$

where U_i is the amplitude of atomic motion upon particular vibration ω_i, the exponential term is known as the Debye–Waller factor, and U_{total} is the mean square displacement of the molecule whose magnitude is in part determined by its thermal motion; hence, it can be reduced by cooling the sample. The incoherent neutron scattering cross section (σ_{inc}) is an isotope-specific property, which does not depend on the chemical environment. As the cross-section value for hydrogen (∼80 barns) is far greater than that for all other elements (typically ca. 5 barns), the INS spectrum emphasizes the modes that involve substantial hydrogen motion.[58] Despite the advantage of INS spectroscopy to study the low-wavenumber modes, the INS intensities decrease considerably above 1000 cm^{-1} due to reduced statistics arising from a decrease in the thermal neutron flux. Hence, the presented data was limited here to the range below 1200 cm^{-1}.

The experimental temperature-dependent Raman spectra covering the phase transition are presented in Figure 4 against the results of the theoretical calculations. An excellent reproduction of most of the spectral features is found for both polymorphs, allowing for clarifying the nature of the observed spectral differences. The calculated wavenumbers

Table 3. Vibrational Band Assignment in the Range 3500−250 cm^{-1} [a]

RS RT	RS 77K[23]	RS RT[17]	RS RT[15]	INS 35K	CASTEP RS RT ND	CASTEP INS 4K ND	Tentative Assignment	RS RT	RS 0.5 GPa[17]	RS 0.7 GPa[15]	INS 35K	CASTEP RS RT ND	CASTEP INS 4K ND	Tentative Assignment
α-resorcinol								**β-resorcinol**						
								3074	3073	3073		See the text		ν_{ss}O-H
3072	3074	3073	3075		See the text		νC-H	3065	3067					νC-H
3057	3060	3058	3061				ν_{ss}O-H	3053	3056	3056				
3045	3046	3045	3049				νC-H	3041	3045	3045				
1626	1618	1614	1612		1621-1608		ν(C=C)	1618	1619	1619		1610-1606		ν(C=C)
1611	1613	1609	1604		1605-1593		δ(O-H···O)	1607	1610	1607		1602-1589		δ(O-H···O)
1510					1504 [A2]		β(C-H); δ(O-H···O)	1506				1494 [B1]		β(C-H); δ(O-H···O)
1316	1311				1343 [A1]			1309				1338 [A1]		
1296					1340 [A1]		δ(O-H···O); β(C-H)	1302				1317 [A1]		δ(O-H···O); β(C-H)
1281					1283 [A1]		β_1(Ph); ν(C-O); β(C-H)	1277				1279 [A1]		β_1(Ph); ν(C-O); β(C-H)
1233					1248 [B1]		β(C-H); δ(O-H···O)	1225				1238 [A1]		β(C-H); δ(O-H···O)
1167				1171	1159 [A1]	1150 [B2]	β(C-H)	1159	1162	1160	1164	1154 [A1]	1142 [B2]	β(C-H)
1145	1165	1163			1143 [B1]			1152	1148	1148		1137 [B1]		
1086	1092	1088	1089	1092	1082 [A1]	1093 [B2]		1080	1082	1085	1088	1075 [A1]	1069 [B2]	
999	1001		993		985 [A2]	986 [A2]	β_1(Ph)	998		998	1004	987 [B2]	988 [B2]	β_1(Ph)
987			978		974 [A1]	963 [B1]	γ(C-H); γ(O-H···O)	987			968	960 [A1]	958 [B2]	γ(C-H); γ(O-H···O)
959	954				951 [A1]		β_2(Ph)	962				955 [A1]		β_2(Ph)
					946	929 [B2]	γ(O-H···O)					925	890 [B1]	γ(O-H···O)
					859	838 [B1]						870	855 [A2]	
					824	815 [A2]	γ(C-H)					819	833 [A2]	γ(C-H)
767				770	762 [A1]	756 [B2]		770			776	764 [A1]	763 [B2]	
				748		739 [B1]	β(C-C-C) + ν(C-O)				742		724 [A2]	β(C-C-C) + ν(C-O)
741	743		745		739 [B1]			745		741		742 [A1]		
686				691	676 [A1]	676 [A1]	T_1(Ph)	687			690	683 [A1]	677 [A1]	T_1(Ph)
615	617	615		618	611 [A1]	610 [B1]	T_2(Ph)	612		614	609	614 [A2]	613 [B2]	T_2(Ph)
560		543	546	548	546 [B1]	546 [B2]	β(C-C-C)	555	547		545	540 [B1]	531 [B2]	β(C-C-C)
542	544	538	541		536 [A1]			542	541	540		534 [A1]		
533	535	531	533	534	525 [A2]	528 [B2]		527	526	527	527	522 [B1]	520 [B2]	
				503		501 [B2]	β(O-C-C)				505		505 [B2]	β(O-C-C)
463	467	463	463	469	454 [A2]	457 [B2]	β(O-C-C); γ(C-C-C)	457		460	458	450 [A1]	457 [B2]	β(O-C-C); γ(C-C-C)
419	422				446 [A2]									
				414		413 [B1]								
383	387			391	394 [B2]	396 [B2]	β(O-C-C)	394			400	408 [A1]	405 [B1]	β(O-C-C)
				379		365 [A1]					369		363 [A2]	
359	360		362		366 [A1]			361		357		370 [B2]		
											300		296 [B2]	
255	253	254	257	260	260 [A1]	242 [A1]	T_3(Ph); γ(O-C-C)	259	261	256	269	264 [A2]	268 [A2]	T_3(Ph); γ(O-C-C)
245	246	246	249	249	244 [A1]	246 [A1]		251	252	247	252	248 [B1]	248 [A1]	

[a]The experimental FT-RS data, collected at room temperature (RT), are presented against the results reported in refs 15, 17, and 23. The theoretical results (CASTEP/PBE/1200 eV) correspond to the computations performed at both high- (RT ND) and low-temperature (4 K ND) cell constants. All of the theoretical wavenumbers were left unscaled. ν, stretching; β, in-plane bending; ω, wagging; T, torsion; β_1, phenyl ring (Ph) trigonal deformation; β_2, antisymmetric deformation type 1; β_3, antisymmetric deformation type 2; T_1, puckering mode; T_2, antisymmetric torsion type 1; T_3, antisymmetric torsion type 2.

(standard PBE) are collected against the experimental data in Table 3 as focusing on the intramolecular phonons.

As the studied phase change is classified as the first-order transition, the order parameter abruptly jumps to a finite value at the critical temperature (T_c), where the free energy of the β-phase accidentally becomes lower than that of the α-structure. As a consequence, the mode softening is not expected and the spectra remain insensitive to temperature, without disclosing any pretransitional effects. However, the spectrum abruptly changes at the α → β transition. The experimental spectra stay in agreement with the results reported in refs 12−18. The most prominent spectral differences are discussed in detail by focusing on different wavenumber areas.

3500−2000 cm^{-1}. The bands due to the νC−H stretching modes arise in the range 3100−3000 cm^{-1}. The νO−H stretching vibrations are believed to be found in the same wavenumber range in both phases, as being lowered in the crystal phase due to the hydrogen bonding of similar strength. The gas-phase spectrum reveals the νO−H bands at 3654 and 3651 cm^{-1}.[24] The reproduction of the highest-energy phonons

is, however, a weak point of our calculations, since the quoted transitions could not be properly predicted with the static harmonic approach. Nevertheless, Balan et al.[59] have already disclosed the effect of lucky cancellation of errors in prediction of the quoted modes by quasi-harmonic GGA calculations.

The experimental Raman spectrum of the α-form reveals the bands at 3072, 3057, and 3045 cm^{-1}, respectively, while the bands at 3074, 3065, 3053, and 3041 cm^{-1} are found in the β-phase.

Although the energy of the νC−H vibrations has been reproduced reasonably, our results are still questionable for the νO−H vibrations, which are strongly affected by the H-bonding. In addition, we have also observed a significant overestimation of the νO−H Raman intensities, which makes the assignment problematic.

Recently, we have faced similar problems with description of the high wavenumber range of many other hydrogen bonded organic crystals, where the Raman silent νO−H stretchings are predicted with a large overestimation of the intensity.[60] Nevertheless, the rPBE calculations seem to provide some
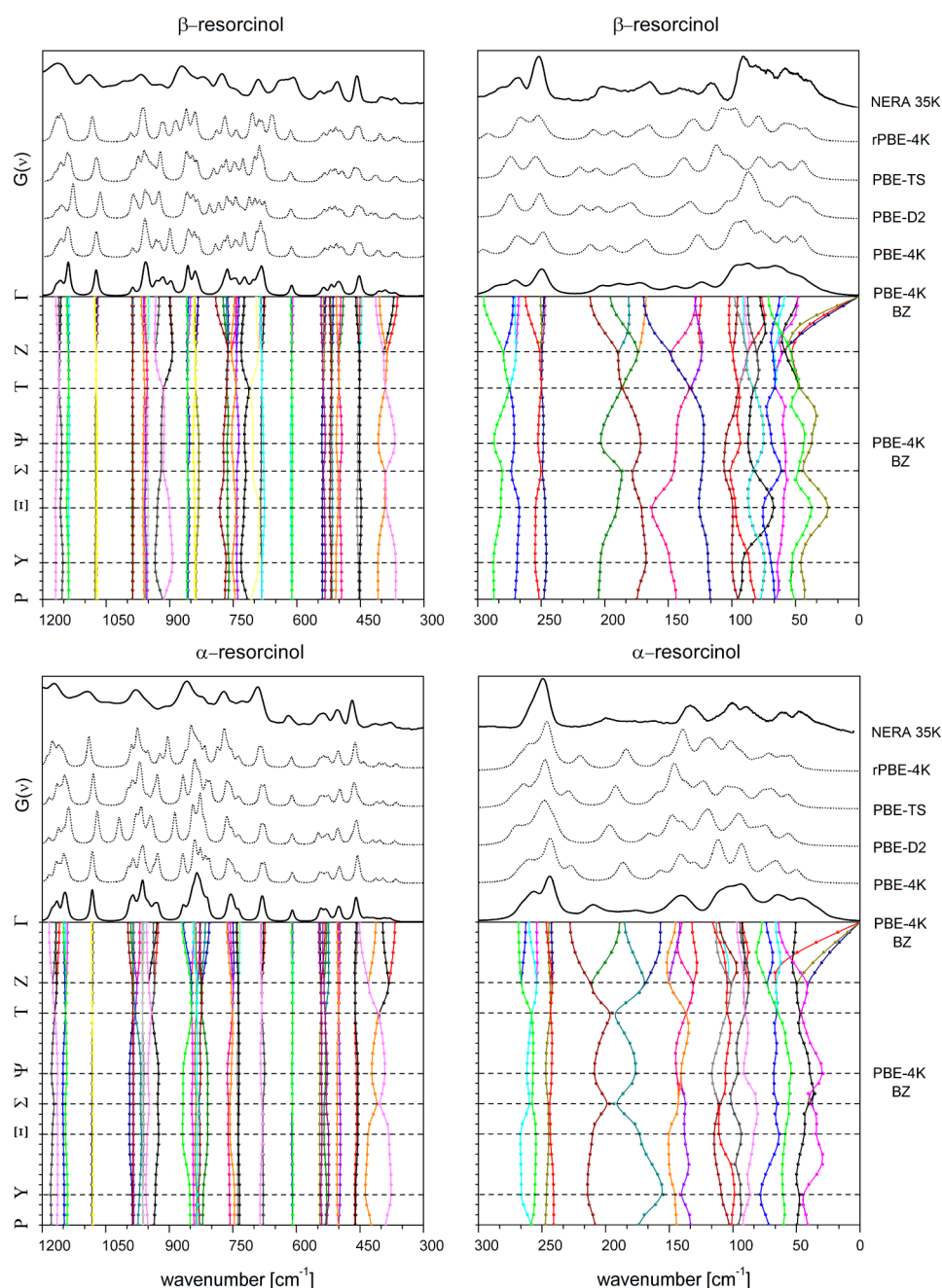
Figure 5. Experimental INS spectra of α- and β-resorcinol, as divided into the range of 1200−300 cm^{-1} and 300−0 cm^{-1}, presented against the results of the plane-wave DFT computations (CASTEP/GGA/1200 eV). The theoretical spectra were calculated at the 4K cell constants and for fully optimized crystal structures with semiempirical vdW corrections. The theoretical spectra were calculated at the Γ-point and averaged by the dispersion throughout the Brillouin zone (BZ).

support, reflecting the advantage of using the "hard" GGA in this field.

The highest energy phonons are described by "hard" and standard GGA as the antisymmetric νO−H stretchings. The related modes are predicted by PBE calculations in the range ∼3235−3130 cm^{-1} in both phases (∼3330−3190 cm^{-1} with rPBE). The quoted results correspond well with a broad FT-IR band, reported for the α-form at 3240 cm^{-1}.[23]

The wavenumbers of the symmetric νO−H modes were found to be strongly functional-dependent as varying in the range 3200−2775 cm^{-1}. The related wavenumbers shift downward for ∼300 cm^{-1} if turning from "hard" to "soft" GGA. It should also be mentioned that the calculations

performed with an inclusion of the vdW corrections did not give any advantage, as being further shifted down with respect to PBE and PW91 (approximately for −40 cm^{-1} with TS, −75 cm^{-1} with D2, and −275 cm^{-1} with OBS).

Ebisuzaki et al.[12] have assigned the band at 3057 cm^{-1} as a νO−H stretching mode by comparing the Raman spectra of proton and deuterated forms of α-resorcinol. The rPBE calculations support this assignment, as predicting the symmetric vibration at 3105 cm^{-1}. It suggests the presence of a slightly stronger H-bonding in the α-phase, since the same mode was predicted at 3202 cm^{-1} for the β-structure. The upward shift may clarify the reason why an additional shoulder was found experimentally at 3074 cm^{-1} in the β-phase

spectrum, while the band at 3057 cm^{-1} vanishes upon the transition, uncovering a νC−H feature.

2000−1200 cm^{-1}. A double feature was found around ∼1610 cm^{-1} in the Raman spectra of both phases as corresponding to the set of the ring stretching modes ν(C= C)Ph, visibly coupled to the δ(COH) vibrations. In the α-phase, two components were observed at 1626 and 1611 cm^{-1}, transforming into the bands at 1618 and 1607 cm^{-1} at the T_c. In the β-phase, the higher band grows in intensity. The factor group splitting implicates eight nondegenerated wavenumbers to be expected in both phases ($\Gamma = 2B_1 + 2B_2 + 2A_1 + 2A_2$). The PBE calculations distribute four upper modes over the range 1621−1608 cm^{-1}, while the set of lower modes is predicted within 1605−1598 cm^{-1}. The calculations properly describe the red-shift down to 1610−1606 and 1602−1589 cm^{-1}, respectively.

The 1600−1200 cm^{-1} range was omitted in the previous literature reports. A very weak band can be found at 1510 cm^{-1}, which slightly shifts down to 1506 cm^{-1} at the phase change. The mode is due to the coupling of the in-plane δ(C−H) bending modes with the δ(O−H···O) deformations and the ν(C=C)Ph stretchings. The PBE calculations predict that, among four modes, the A$_2$ symmetry species gives a dominant contribution to the band intensity in α-resorcinol, being predicted at 1504 cm^{-1}, while the B$_1$ mode dominates in the β-form, being predicted at 1494 cm^{-1}.

1200−250 cm^{-1}. The range beneath 1200 cm^{-1} has been supported by INS spectroscopy. Nevertheless, the INS resolution above ∼600 cm^{-1} is still much lower if compared to Raman spectroscopy. In Figure 5, the experimental amplitude-weighted density of vibrational states $G(\nu)$ spectra are presented against the representative results of the plane-wave DFT calculations.

The simplicity of the INS intensity expression allows one to overcome the technical limitations of the linear-response implementation. Hence, with the help of the finite-displacement approach, we were able to impose the vdW corrections, illustrating their influence on the vibrational spectrum.

As the hydrogen-bonding framework is not limited to the unit-cell level, one may note a significant phonon dispersion, which should not be ignored in the simulations, especially if referring to the low-energy transfer range. The reported INS spectra were hence simulated both at the Γ-point (dotted) and averaged by phonon dispersion (BZ).

One of the most prominent differences in the Raman spectrum is related to the band at ∼1150 cm^{-1}, assigned to the set of β(C−H) bending modes. The calculations predict the red-shifting of the B$_2$ symmetry species from 1150 cm^{-1} (α) down to 1142 cm^{-1} (β). The nature of this change is interesting as being related to the molecular shifting. In the α-phase, there is a kind of T-shaped stacking of the neighboring molecules. The molecules are further shifted and slightly reoriented at the transition, what results in stronger interactions between the C−H pairs and the π electrons. The attracting interactions shift down the phonon wavenumbers and affect the polarizability, giving rise to the Raman response. The barely visible bands found at 1167 (A$_1$) and 1145 cm^{-1} (B$_1$) are then clearly observed at 1159 and 1152 cm^{-1}, respectively. A similar effect was observed in the case of a medium-intensity A$_1$ symmetry β(C−H) band, which was observed in the FT-RS spectrum at 1086 cm^{-1} (α-phase) and 1080 cm^{-1} (β-phase). The red-shifted band was properly described by theory at 1082 and

1075 cm^{-1}, respectively. The downward shift is also triggered by the attracting interactions.

The most intense FT-RS band is found near 1000 cm^{-1}, being clearly assigned to the trigonal deformation of the phenyl ring β_1(Ph). As the related mode is localized on the ring framework, it is not affected by the phase transition.

The Raman spectrum is nearly silent in the range ∼1000−750 cm^{-1}. On the contrary, the INS spectrum is densely covered by the out-of-plane vibrations involving a substantial hydrogen motion. The discussed vibrations are generally due to the γ(C−H) bendings, mixed with the γ(O−H···O) modes. As the γ(O−H···O) motions disturb the infinite H-bond networks, the bands are significantly affected by phonon dispersion, giving an additional broadening of the INS bands. As may be deduced from Figure 5, the modes in the range ∼1000−700 cm^{-1} strongly depend on the theory level and the use of the vdW corrections.

The medium-intensity band, found in the FT-RS spectrum at 741 cm^{-1} (α-phase) and blue-shifted up to 745 cm^{-1} at the transition, can be assigned to the β(C−C−C) ring deformation coupled to the ν(C−O) stretching modes, which affect the networks of the hydrogen bonds, giving poorly resolved INS signals.

A clear difference between both polymorphs manifests in the set of weak bands found in the FT-RS spectra at 560, 542, and 533 cm^{-1} (α-phase) and 555, 542, and 527 cm^{-1} (β-phase). The related bands were observed by INS at 548, 534 cm^{-1} (α-phase) and 545, 527 cm^{-1} (β-phase), respectively. The discussed modes are dominated by the β(C−C−C) deformations. A well resolved band, found in the INS spectrum at 503 (α-phase) and 505 cm^{-1} (β-phase), respectively, can be assigned to the similar β(O−C−C) vibrations. The well resolved INS band, assigned to the mixed β(O−C−C)/γ(C−C−C) deformations can also be found at 469 (α-phase) and 458 cm^{-1} (β-phase), while being barely visible in FT-RS at 463 and 457 cm^{-1}, respectively.

Clear evidence of the spectral differences has also been provided by the theoretical calculations with the set of modes contributing to the INS and FT-RS spectra in the range ∼420−350 cm^{-1}. The modes are linked to the β(O−C−C) localized vibrations, significantly affecting the H-bonding network. The related calculations properly define the spectral intensity differences in both Raman and INS spectroscopy.

Further spectral differences are manifested in the bands assigned to the γ(O−C−C) deformations, coupled with the torsional ring deformations and observed by FT-RS at 255, 245 cm^{-1} (α-phase) and 259, 251 cm^{-1} (β-phase). The related modes contribute to the INS spectrum at 260, 249 cm^{-1} (α-phase) and 269, 252 cm^{-1} (β-phase). The phonon dispersion, which is more prominent in the β-form, leads to several additional features observed throughout ∼300−270 cm^{-1}.

Low-Wavenumber Range <250 cm^{-1}. The low-wavenumber range reveals striking spectral differences. Among the 165 zone-center phonons, 21 are the external modes, spanned beneath 200 cm^{-1}.

The temperature dependence of the low-wavenumber Raman spectrum has been earlier studied by Ebisuzaki[12] and by Shigenari et al.[13,14] The authors have also noticed that the mode wavenumbers change suddenly at T_c and then again become insensitive to temperatures above T_c. It was concluded by Shigenari et al.[13,14] that, even in the first-order transitions, the crystal-phase reorganization would not occur all at once over a macroscopic range, but local nucleations of the new

Table 4. Vibrational Band Assignment in the Wavenumber Range below <250 cm^{-1} [a]

RS			THz		INS 35K	CASTEP PBE		Tentative Assignment	RS			THz RT	INS 35K	CASTEP PBE		Tentative Assignment
FT RT	77K[23]	RT[17]	RT	RT[63]		RT ND	4K ND		FT RT	0.5 GPa[17]	0.7 GPa[15]	RT		RT ND	4K ND	
α-resorcinol									β-resorcinol							
Lattice Modes																
					200		227.0 [A$_1$]						202		211.6 [B$_2$]	
195	195	198				223.0 [A$_1$]		T_3(Ph); νO···O	197						207.6 [B$_2$]	T_3(Ph); νO···O
													193		195.7 [A$_2$]	
				179			185.2 [B$_1$]						183		181.3 [A$_1$]	
									180			171			191.0 [A$_2$]	
164	163	164			163	153.7 [A$_2$]	156.9 [A$_2$]	ν_{ss}O···O					164		167.4 [B$_1$]	ν_{ss}O···O
													156		169.3 [A$_1$]	νO···O
137				134		139.0 [B$_1$]	141.5 [B$_1$]	ρPh ; νO···O	145					160.4 [B$_1$]		ρPh ; νO···O
				127		132.3 [A$_1$]		ωPh ; νO···O					139		128.1 [B$_1$]	ωPh ; νO···O Dispersed
118	116	120	114.0	111.0		126.4 [A$_1$]		ωPh ; νO···O					117		124.3 [A$_1$]	ωPh ; νO···O
			110				115.9 [B$_2$]		110	113				119.7 [A$_1$]		
				101			110.8 [A$_2$]					110			123.5 [B$_2$]	
101	102	105	99.6	98.5		109.0 [A$_1$]										
				89			93.0 [B$_1$]						90		98.0 [B$_2$]	
83	84	85	84.0	80.0		90.4 [B$_2$]		ωPh	79	82				83.6 [A$_1$]		ωPh
						91.9 [A$_2$]							80		78.0 [A$_1$]	
								←Ph→; ←O··H···O→				74.1		79.2 [B$_2$]		
													70		71.5 [A$_2$]	←Ph→; ↑O··H···O↑
			62.6	61.0		72.5 [B$_1$]			60	61				67.6 [A$_2$]		
60	58	60	59.4	57.8	61	65.8 [B$_2$]	64.3 [B$_2$]	←Ph→; δO··H···O					58		62.5 [A$_2$]	
			55.0	54.7		65.1 [A$_1$]		←Ph→; δO··H···O				51.6		58.0 [B$_1$]	58.5 [B$_1$]	←Ph→; δO··H···O
													44	43.3 [B$_2$]	48.1 [B$_2$]	
	46	47			48	50.7 [A$_2$]	50.6 [A$_2$]	←Ph→; ↑O··H···O↑	39[14]			37	49	37.4 [A$_1$]	47.9 [A$_1$]	←Ph→; ↑O··H···O↑
					29			Dispersion /Acoustic					32			Dispersion /Acoustic

[a] The experimental FT-RS and THz data at room temperature are presented against the data reported in refs 14, 15, 17, 23, and 63. The theoretical results (CASTEP PBE) correspond to the computations performed for both high-temperature (RT ND) and low-temperature (4 K ND) structures as referring to the Raman, TDs-THz, and INS experimental conditions. All of the theoretical wavenumbers were left unscaled. ←Ph→, molecular translations; ρPh, molecular screwing modes; ωPh, molecular wagging modes; νO···O, H-bond bridge stretching; δO··H···O, H-bond deformation; ↑O··H···O↑, breathing modes; ←O··H···O→, shearing modes.

phase would appear at the temperatures far from T_c. Hence, although there is no mode-softening expected, the nucleation may be preceded by the momentary but large-amplitude fluctuations of molecular vibrations. This idea was further explored with the help of the polarized fluorescence-lifetime measurements, where it was concluded that a highly excited A_2 symmetry mode must be responsible for the critical shortening of the fluorescence lifetime, which was assumed to be the phase-transition precursor. Hence, one may expect that large displacements and reorientations of the molecules would give rise to a nucleation of the β-phase. It is hence interesting to look at the nature of the low-wavenumber modes.

As has been shown in the Supporting Information, the isolated molecule calculations cannot give any support to the interpretation, since the lowest-energy vibrations are expected at ca. 215 cm^{-1} (see Table S1 and Figure S2, Supporting Information). The final answer can only be delivered by imposing the periodic boundary conditions. Furthermore, the related INS bands are strongly affected by phonon dispersion, which should be further taken into account. It should also be noted that the calculations of the low-energy transfer range are challenging from the technical point of view, since all the numerical errors accumulate here. Some notes on the precise plane-wave DFT calculations of the terahertz range were presented by Jepsen and Clark in ref 61. The calculations reported here have followed the given receipt. Nevertheless, it should be noted that the derivatives of the Fourier series need more terms to converge accurately. Hence, in addition to accurate plane-wave and k-point grid convergence, one needs to use a much larger basis size for the description of the charge density. Most of the plane-wave codes use the so-called "double-grid" technique, with a finer fast Fourier transform (FFT) grid defined by a second cutoff energy.[62] In CASTEP, a dimensionless coefficient was used in order to multiply the baseline size by a factor of 6.0. Such extreme conditions allowed us to minimize the wavenumber oscillations and deliver well-converged results, with a quality comparable to the above quoted full-electronic calculations.[40]

By analyzing Figure 5, one can observe the influence of the vdW corrections on the low-wavenumber range. The theoretical wavenumbers slightly shift upward upon inclusion of the semiempirical corrections. It is interesting to note that, while the low-range PBE-D2 spectra are close to the PBE results, the PBE-TS calculations are very comparable to rPBE.

The collection of the related experimental wavenumbers has been given in Table 4. For the visualization of the related modes, we refer the reader to the Supporting Information. The range above 130 cm^{-1} is linked to the eight νO···O stretching modes, slightly mixed with the energetically lowest ring deformations, giving very weak Raman signals. The O···O stretching character dominates when going down in the wavenumber scale. The remaining modes cover the range
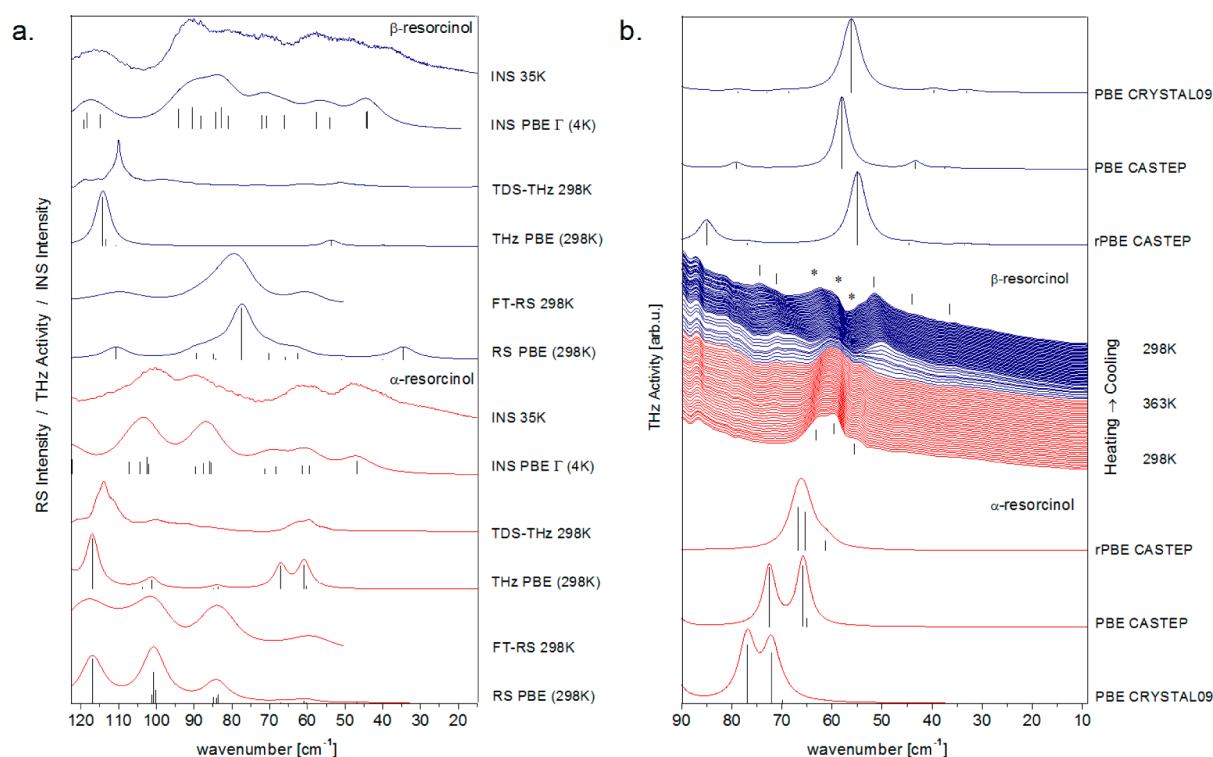
Figure 6. Collection of the low-wavenumber complementary experimental data (FT-RS, TDS-THZ, INS) for α- and β-resorcinol as presented against the results of the theoretical CASTEP PBE calculations at the Γ-point (a). Note that the theoretical wavenumbers were multiplied by an empirical factor of 0.925. Part b collects the temperature-dependent TDS-THz spectra covering the phase transition, presented in the range below 90 cm^{-1}, against the theoretical results obtained with CASTEP and CRYSTAL09 at the room-temperature volume. All the wavenumbers were left unscaled. Note that some trails of the α-form, observed due to a very low absorbance of the β-form, are denoted with an asterisk.
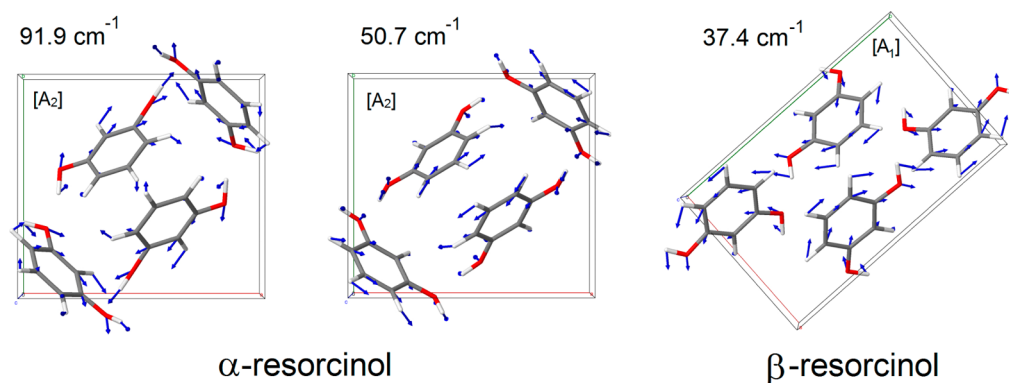
Figure 7. Visualization of selected low energy phonon modes (A_2 and A_1 symmetry) in α- and β-resorcinol according to the CASTEP/PBE calculations with the theoretical wavenumbers given.

below <125 cm^{-1}, which can be further explored by combining INS and Raman (down to the notch filter limit) with the TDs-THz spectroscopy.

The experimental data are presented against the results of the PBE calculations in Figure 6a. It should be noted that a systematic overestimation of the calculated wavenumbers was found in the whole range below ~150 cm^{-1}. Recently, we have experienced a similar ~10% overestimation in the case of another hydrogen-bonded molecular crystal.[60] Hence, for better transparency, we have empirically rescaled the calculated wavenumbers by a factor of 0.925 while keeping the data in Table 4 unscaled.

The temperature-dependent terahertz spectra covering the $\alpha \rightarrow \beta$ transition has been presented in Figure 6b, as focusing on the range below 90 cm^{-1}. By comparing parts a and b of Figure

6, one may observe a very weak absorption in the β-phase, which makes the related bands barely detectable. The experimental data has been given against the results of the solid-state DFT calculations, both employing the plane waves and atomic-centered basis sets. The comparison of the pseudopotential and the full-electronic results confirms a highly accurate convergence of the CASTEP results. It should be noted that the terahertz spectrum of the α-phase has already been reported by Zheng et al.,[63] where the spectral analysis was supported by CASTEP calculations, following the procedure suggested by Jepsen and Clark.[61] The experimental results presented here stay in agreement with the reported data. However, our computational results definitely stay in conflict with the reported calculations.[63] When comparing these results, one may notice a completely different relation of the

wavenumbers (see Figure 6b). We believe that such a discrepancy can be possibly linked to the numerical noise coming from a bad description of the Fourier series derivatives.

By analyzing the figure, one may clearly see a remarkable agreement between the theoretical and experimental data, which confirms a high credibility of the computational results.

According to Figure 6a, one may observe a relatively intense feature at $\sim$115 cm^{-1} in the THz and Raman spectra of the α-phase. The band shifts down to $\sim$110 cm^{-1} at the critical point and can be assigned to the wagging-like resorcinol reorientation, slightly mixed with the νO$\cdots$O stretchings. The bands of similar nature, observed in the INS spectrum, shift down from 127 to 115 cm^{-1} upon the structural transformation. The set of similar bands contributes to the α-phase spectra at $\sim$100 cm^{-1}, while giving a shoulder signal in the INS spectrum of the β-phase, observed at $\sim$90 cm^{-1}.

In order to facilitate the discussion, several low-wavenumber modes have been visualized in Figure 7. The relatively well-resolved bands observed in the optical spectra at $\sim$80 cm^{-1} are of complex nature, being dominated by the localized out-of-plane molecular reorientations. The range below <80 cm^{-1} can be assigned to the phonon modes engaging the molecular translations. A complex band, with the peaks at 63, 59, and 55 cm^{-1}, can be found in the TDs-THz spectrum of the α-phase. The middle counterpart also contributes to the Raman spectrum at 60 cm^{-1}.

The α-phase calculations predict the energetically lowest mode at 50.7 cm^{-1} (see Figure 7), which is in principle allowed in Raman spectroscopy. Due to the technical limitations, we were not able to observe this band, which, however, has already been reported in the literature at 46 and 47 cm^{-1}.[23,17] Its presence was also confirmed by INS at 48 cm^{-1}.

At the transition, a very weak band emerges in the TDs-THz spectrum at 52 cm^{-1}. The theory predicts the transition at 58 cm^{-1} (B$_1$ symmetry). Another band is detected with extremely low intensity at 44 cm^{-1}, while being predicted at 43 cm^{-1} (B$_2$ symmetry). The theory gives one transition more, expected at 37.4 cm^{-1} (see Figure 7), which is supposed to be found at 37 cm^{-1} at the noise level. The latter mode is predicted to be significantly Raman active, which unfortunately cannot be verified in our experiment due to the notch cutoff at 50 cm^{-1}. Nevertheless, the band was clearly observed, e.g., by Shigenari et al.[14] The quoted mode also contributes to the INS band at 49 cm^{-1}. The theory also predicts its wavenumber to be shifted up to 48 cm^{-1}, if turning to the low-temperature cell parameters.

The low-wavenumber modes shown in Figure 7 are easily populated by thermal activation. As mentioned, one may expect that large displacements and reorientations of the molecules would give rise to the nucleation of the β-phase. The analysis of the eigenvectors suggests that the A$_2$ symmetry species can provide a direct nucleation pathway. Unfortunately, one should note that the A$_2$ are silent in TDs-THz as the symmetry-forbidden transitions, while being barely detectable by Raman spectroscopy.

By analyzing the low-energy transfer INS spectra, one may also note the presence of the lowest features in both phases at $\sim$30 cm^{-1}, which can be attributed to the highly dispersed acoustic modes.

CONCLUSIONS

The polymorphism of resorcinol has been extensively explored by combining optical and neutron spectroscopy with theoretical calculations in periodic boundary conditions. Despite the quasi-harmonic methodology, it was found that the calculations in the frame of standard and "hard" formulation of the generalized gradient approximation were able to successfully reproduce the whole spectral range, allowing for a detailed interpretation of the vibrational bands. The computations provide an insight into the nature of the spectral differences observed by each spectroscopy. As the hydrogen-bond network is not saturated at the unit-cell level, the calculations predict significant phonon dispersion in the system. The inclusion of the phonon dispersion was found to be essential in the description of most characteristic INS features. The most striking spectral differences were found in the low-wavenumber range, which is interpreted on the basis of highly reliable theoretical data.

ASSOCIATED CONTENT

Ⓢ Supporting Information

Figures showing the crystal structures of the α and β polymorphic forms of resorcinol and theoretical Raman spectra of the α and β conformers of resorcinol. Tables showing full normal coordinate analysis of the α and β conformers, visualization of the low-wavenumber phonons calculated at the Γ-point, and collection of the theoretical wavenumbers, infrared activities, and Raman intensities. This material is available free of charge via the Internet at http://pubs.acs.org.

AUTHOR INFORMATION

Corresponding Author
*E-mail: kacper.druzbicki@amu.edu.pl.
Notes
The authors declare no competing financial interest.

REFERENCES

(1) Robertson, J. M. The Structure of Resorcinol A Quantitative X-Ray Investigation. *Proc. R. Soc. A* **1936**, *157*, 79−99.

(2) Robertson, J. M.; Ubbelohde, A. B. A New Form of Resorcinol. I. Structure Determination by X-Rays. *Proc. R. Soc. A* **1938**, *167*, 122−135.

(3) Durairaj, R. B. *Resorcinol: Chemistry, Technology, and Applications*; Springer: Berlin, Heidelberg, 2005.

(4) Dressler, H. *Resorcinol: Its Uses and Derivatives*; Plenum Press: New York, 1994.

(5) Pelzl, G.; Wirth, I.; Weissflog, W. The First 'Banana Phase' Found in an Original Vorländer Substance. *Liq. Cryst.* **2001**, *28*, 969−972.

(6) Pelzl, G.; Diele, S.; Weissflog, W. Banana-Shaped Compounds—A New Field of Liquid Crystals. *Adv. Mater.* **1999**, *11*, 707−724.

(7) Sadashiva, B. K.; Raghunathan, V. A.; Pratibha, R. Evidence of Columnar Structure in Compounds Composed of Banana-Shaped Molecules. *Ferroelectrics* **2000**, *243*, 249−260.

(8) Weissflog, W.; Nadasi, H.; Dunemann, U.; Pelzl, G.; Diele, S.; Eremin, A.; Kresse, H. Influence of Lateral Substituents on the Mesophase Behaviour of Banana-Shaped Mesogens. *J. Mater. Chem.* **2001**, *11*, 2748−2758.

(9) Bacon, G. E.; Jude, R. J. Neutron-Diffraction Studies of Salicylic Acid and α-Resorcinol. *Z. Kristallogr.* **1973**, *138*, 19−40.

(10) Bacon, G. E.; Lisher, E. J.; Pawley, G. S. A Neutron Powder Diffraction Study of Deuterated α-Resorcinol: a Test of Profile Refinement Using TLS Constraints. *Acta Crystallogr., Sect. B* **1979**, *35*, 1400−1403.

(11) Bacon, G. E.; Lisher, E. J. A Neutron Powder Diffraction Study of Deuterated α- and β-Resorcinol. *Acta Crystallogr., Sect. B* **1980**, *36*, 1908−1916.

(12) Ebisuzaki, Y.; Askari, L. H.; Bryan, A. M.; Nicol, M. F. Phase Transitions in Resorcinal. *J. Chem. Phys.* **1987**, *87*, 6659−6664.

(13) Shigenari, T.; Kojima, E.; Ino, Y.; Abe, K. Detection of a Precursor in a Strong First-Order Structural Phase Transition by a Fluorescence-Lifetime Measurement. *Phys. Rev. Lett.* **1991**, *66*, 2112−2115.

(14) Shigenari, T.; Abe, K.; Morita, K.; Pingm, Qi.; Kojima, E.; Ino, H. Precursor of a Strong First-Order Phase Transition: Critical Speeding-Up of Fluorescence Lifetime in the α - β Transition of Resorcinol. *J. Phys.: Condens. Matter* **1994**, *6*, 7469−7482.

(15) Kichanov, S. E.; et al. The Polymorphic Phase Transformations in Resorcinol at High Pressure. *J. Mol. Struct.* **2011**, *1006*, 337−343.

(16) Deb, S. K.; Rekha, M. A.; Roy, A. P.; Vijayakumar, V.; Meenakshi, S.; Gudwal, B. K. Raman-Scattering Study of High-Pressure Phase Transition and Amorphization of Resorcinol. *Phys. Rev. B* **1993**, *47*, 11491−11494.

(17) Rao, R.; Sakuntala, T.; Godwal, B. K. Evidence for High-Pressure Polymorphism in Resorcinol. *Phys. Rev. B* **2002**, *65*, 054108−054116.

(18) Rao, R.; Sakuntala, T.; Arora, A. K.; Deb, S. K. Pressure Induced Phase Transitions in Hydroquinone. *J. Chem. Phys.* **2004**, *121*, 7320−7325.

(19) Penot, D.; Mathieu, J. P. Spectre Raman des Cristaux de Résorcine α et β. *J. Chim. Phys. Phys.-Chim. Biol.* **1955**, *52*, 829−833.

(20) Hidalgo, A.; Otero, C. Infrared Absorption Spectra of the Diphenols and Phenol. *Spectrochim. Acta* **1960**, *16*, 528−539.

(21) Green, J. H. S. Vibrational Spectra of Benzene Derivatives—VIII. m-Disubstituted Compounds. *Spectrochim. Acta, Part A* **1970**, *26*, 1523−1533.

(22) Green, J. H. S.; Harrison, D. J.; Kynaston, W. Vibrational Spectra of Benzene Derivatives—XIV: Mono Substituted Phenols. *Spectrochim. Acta, Part A* **1971**, *27*, 2199−2217.

(23) Tripathi, G. N. R. Crystal Spectra and Vibrational Assignments in α-Resorcinol. *J. Chem. Phys.* **1981**, *74*, 250−255.

(24) Gerhards, M.; Perl, W.; Kleinermanns, K. Rotamers and Vibrations of Resorcinol Obtained by Spectral Hole Burning. *Chem. Phys. Lett.* **1995**, *240*, 506−512.

(25) Imhof, P.; Brause, R.; Kleinermanns, K. Determination of Ground State Vibrational Frequencies of Jet-Cooled Resorcinol by Means of Dispersed Fluorescence Spectroscopy and ab Initio Calculations. *J. Mol. Spectrosc.* **2002**, *211*, 65−70.

(26) Natkaniec, I.; Bragin, S. I.; Brankowski, J.; Mayer, J. In Steigenberger, U., Broome, T., Ress, G., Soper, A., Eds. Proceedings of the XIIth Meeting on International Collaboration on Advanced Neutron Sources, Rutherford Appleton Laboratory Report 1994, *1*, 94−025.

(27) Clark, S. J.; Segall, M. D.; Pickard, C. J.; Hasnip, P. J.; Probert, M. J.; Refson, K.; Payne, M. C. First Principles Methods Using CASTEP. *Z. Kristallogr.* **2005**, *220*, 567−570.

(28) Rappe, A. M.; Rabe, K. M.; Kaxiras, E.; Joannopoulos, J. D. Optimized Pseudopotentials. *Phys. Rev. B* **1990**, *41*, 1227−1230.

(29) Andzelm, J.; King-Smith, R. D.; Fitzgerald, G. Geometry Optimization of Solids Using Delocalized Internal Coordinates. *Chem. Phys. Lett.* **2001**, *335*, 321−326.

(30) Refson, K.; Clark, S. J.; Tulip, P. R. Variational Density-Functional Perturbation Theory for Dielectrics and Lattice Dynamics. *Phys. Rev. B* **2006**, *73*, 155114−155136.

(31) Baroni, S.; Giannozzi, P.; Testa, A. Green's-Function Approach to Linear Response in Solids. *Phys. Rev. Lett.* **1987**, *58*, 1861−1864.

(32) Gonze, X.; Allan, D. C.; Teter, M. P. Dielectric Tensor, Effective Charges, and Phonons in Neutron-Diffraction Studies of Salicylic Acid and α-Quartz by Variational Density-Functional Perturbation Theory. *Phys. Rev. Lett.* **1994**, *68*, 3603−3606.

(33) Gonze, X. Perturbation Expansion of Variational Principles at Arbitrary Order. *Phys. Rev. A* **1995**, *52*, 1086−1095.

(34) Gonze, X. Adiabatic Density-Functional Perturbation Theory. *Phys. Rev. A* **1995**, *52*, 1096−1114.

(35) Gonze, X. Dynamical Matrices, Born Effective Charges, Dielectric Permittivity Tensors, and Interatomic Force Constants From Density-Functional Perturbation Theory. *Phys. Rev. B* **1997**, *55*, 10337−10354.

(36) Baroni, S.; Dal Corso, A.; de Gironcoli, S.; Giannozzi, P. Phonons and Related Crystal Properties from Density-Functional Perturbation Theory. *Rev. Mod. Phys.* **2001**, *73*, 515−561.

(37) Milman, V.; Perlov, A.; Refson, K.; Clark, S. J.; Gavartin, J.; Winkler, B. Structural, Electronic and Vibrational Properties of Tetragonal Zirconia Under Pressure: a Density Functional Theory Study. *J. Phys.: Condens. Matter* **2009**, *21*, 485404−485416.

(38) Gonze, X.; Charlier, J. C.; Teter, M. P. Interatomic Force Constants from First Principles: The Case of α-Quartz. *Phys. Rev. B* **1994**, *50*, 13035−13038.

(39) Ramirez-Cuesta, A. The New Version of the Software for Analyzing and Interpreting INS Spectra. *Comput. Phys. Commun.* **2004**, *157*, 226−238.

(40) Dovesi, R.; Orlando, R.; Civalleri, B.; Roetti, R.; Saunders, V. R.; Zicovich-Wilson, C. M. CRYSTAL: a Computational Tool for the ab initio Study of the Electronic Properties of Crystals. *Z. Kristallogr.* **2005**, *220*, 571−573.

(41) Perdew, J. P.; Burke, K.; Wang, Y. Generalized Gradient Approximation for the Exchange-Correlation Hole of a Many-Electron System. *Phys. Rev. B* **1996**, *54*, 16533−16539.

(42) Perdew, J. P.; Burke, K.; Ernzerhof, M. Generalized Gradient Approximation Made Simple. *Phys. Rev. Lett.* **1996**, *77*, 3865−3868.

(43) Peintinger, M. F.; Vilela Oliveira, D.; Bredow, T. Consistent Gaussian Basis Sets of Triple-Zeta Valence With Polarization Quality for Solid-State Calculations. *J. Comput. Chem.* **2012**, *34*, 451−459.

(44) Frisch, M. J.; et al. *Gaussian 09*, revision D.1; Gaussian, Inc.: Wallingford, CT, 2009.

(45) Martin, J. M. L.; Van Alsenoy, C. *GAR2PED*; University of Antwerp: Antwerp, Belgium, 1995.

(46) Haas, P.; Tran, F.; Blaha, P.; Schwarz, K. Construction of an Optimal GGA Functional for Molecules and Solids. *Phys. Rev. B* **2011**, *83*, 205117−205123.

(47) Wu, Z.; Cohen, R. E. More Accurate Generalized Gradient Approximation for Solids. *Phys. Rev. B* **2006**, *73*, 235116−235122.

(48) Perdew, J. P.; Ruzsinszky, A.; Csonka, G. I.; Vydrov, O. A.; Scuseria, G. E.; Constantin, L. A.; Zhou, X.; Burke, K. Restoring the Density-Gradient Expansion for Exchange in Solids and Surfaces. *Phys. Rev. Lett.* **2008**, *100*, 136406−136410.

(49) Hammer, B.; Hansen, L. B.; Nørskov, J. K. Improved Adsorption Energetics Within Density-Functional Theory Using Revised Perdew-Burke-Ernzerhof Functionals. *Phys. Rev. B* **1999**, *59*, 7413−7421.

(50) Klimeš, J.; Michaelides, A. Perspective: Advances and Challenges in Treating Van Der Waals Dispersion Forces in Density Functional Theory. *J. Chem. Phys.* **2012**, *137*, 120901−120913.

(51) Ortmann, F.; Bechstedt, F.; Schmidt, W. G. Semiempirical Van Der Waals Correction to the Density Functional Description of Solids and Molecular Structures. *Phys. Rev. B* **2006**, *73*, 205101−205111.

(52) Grimme, S. Semiempirical GGA-Type Density Functional Constructed With a Long-Range Dispersion Correction. *J. Comput. Chem.* **2006**, *27*, 1787−1799.

(53) Tkatchenko, A.; Scheffler, M. Accurate Molecular Van Der Waals Interactions from Ground-State Electron Density and Free-Atom Reference Data. *Phys. Rev. Lett.* **2009**, *102*, 073005−073009.

(54) Tkatchenko, A.; DiStasio, R. A., Jr.; Car, R.; Scheffler, M. Accurate and Efficient Method for Many-Body van der Waals Interactions. *Phys. Rev. Lett.* **2012**, *108*, 236402−236407.

(55) Marom, N.; DiStasio, R. A., Jr.; Atalla, V.; Levchenko, S.; Reilly, A. M.; Chelikowsky, J. R.; Leiserowitz, L.; Tkatchenko, A. Many-Body Dispersion Interactions in Molecular Crystal Polymorphism. *Angew. Chem., Int. Ed.* **2013**, *52*, 6629−6632.

(56) Rivera, S. A.; Allis, D. G.; Hudson, B. S. Importance of Vibrational Zero-Point Energy Contribution to the Relative Polymorph Energies of Hydrogen-Bonded Species. *Cryst. Growth Des.* **2008**, *8*, 3905−3907.

(57) Bret-Dibat, P.; Lichanot, A. Thermodynamic Properties of Positional Isomers of Disubstituted Benzene in Condensed Phase. *Thermochim. Acta* **1989**, *147*, 261−271.

(58) Parker, S. F.; Haris, P. I. Inelastic Neutron Scattering Spectroscopy of Amino Acids. *Spectroscopy* **2008**, *22*, 297−307.

(59) Balan, E.; Lazzeri, M.; Delattre, S.; Méheut, M.; Refson, K.; Winkler, B. Anharmonicity of Inner-OH Stretching Modes in Hydrous Phyllosilicates: Assessment from First-Principles Frozen-Phonon Calculations. *Phys. Chem. Miner.* **2007**, *34*, 621−625.

(60) Łuczyńska, K.; Drużbicki, K.; Łyczko, K.; Starosta, W. Complementary Optical and Neutron Vibrational Spectroscopy Study of Bromanilic Acid: 2,3,5,6-Tetramethylpyrazine (1:1) Cocrystal. *Vib. Spectrosc.* **2014**, *75*, 26−38.

(61) Jepsen, P. U.; Clark, S. J. Precise ab-initio Prediction of Terahertz Vibrational Modes in Crystalline Systems. *Chem. Phys. Lett.* **2007**, *442*, 275−280.

(62) Laasonen, K.; Pasquarello, A.; Car, R.; Lee, C.; Vanderbilt, D. Car-Parrinello Molecular Dynamics with Vanderbilt Ultrasoft Pseudopotentials. *Phys. Rev. B* **1993**, *47*, 10142−10153.

(63) Zheng, Z.-P.; Fan, W.-H.; Yan, H. Terahertz Absorption Spectra of Benzene-1,2-diol, Benzene-1,3-diol and Benzene-1,4-diol. *Chem. Phys. Lett.* **2012**, *525*, 140−143.